Effects of Annealing on the Nanomorphology and Performance of Poly(alkylthiophene):Fullerene Bulk-Heterojunction Solar Cells

ARTICLE *in* ADVANCED FUNCTIONAL MATERIALS · MARCH 2007

Impact Factor: 11.81 · DOI: 10.1002/adfm.200601038

DOI: 10.1002/adfm.200601038

Effects of Annealing on the Nanomorphology and Performance of Poly(alkylthiophene):Fullerene Bulk-Heterojunction Solar Cells**

By *Le Huong Nguyen*,* *Harald Hoppe*,* *Tobias Erb*, *Serap Günes*, *Gerhard Gobsch*, *N. Serdar Sariciftci*

The evolution of nanomorphology within thin solid-state films of poly(3-alkylthiophene):[6,6]-phenyl-C_{61} butyric acid methyl ester (P3AT:PCBM) blends during the film formation and subsequent thermal annealing is reported. In detail, the influence of the P3AT's alkyl side chain length on the polymer/fullerene phase separation is discussed. Butyl, hexyl, octyl, decyl, and dodecyl side groups are investigated. All of the P3ATs used were regioregular. To elucidate the nanomorphology, atomic force microscopy (AFM), X-ray diffraction, and optical spectroscopy are applied. Furthermore, photovoltaic devices of each of the different P3ATs have been constructed, characterized, and correlated with the nanostructure of the blends. It is proposed that the thermal-annealing step, commonly applied to these P3AT:PCBM blend films, controls two main issues at the same time: a) the crystallization of P3AT and b) the phase separation and diffusion of PCBM. The results show that PCBM diffusion is the main limiting process for reaching high device performances.

1. Introduction

Photovoltaic solar cells have attracted much interest in the scientific community because they represent a clean, sustainable energy source that could potentially reduce the dependence on fossil fuels. Organic photovoltaics are expected to benefit from a variety of properties such as low manufacturing energy and costs, light weight, flexibility, and large-scale production volumes compared to conventional photovoltaic devices based on silicon. Recently organic photovoltaic cells with efficiencies of up to 5 % using conjugated polymer blends in a bulk heterojunction concept are reported.[1] In this bulk heterojunction concept[2] the large interfacial area between donor and acceptor phases provides sufficient charge separation as a prerequisite for solar-cell operation. To increase the power-conversion efficiency strong absorption of sunlight as well as efficient charge separation and transport within the interpenetrating networks is required. Exciton dissociation is known to occur at the interface between two materials with different excited-state energy levels presenting an abrupt change in the potential (strong electric fields at the interface).[3] Charge-carrier transport in organic materials can be enhanced by increasing the mesoscopic order and crystallinity.[4] Especially the electronic properties of the individual materials as well as the morphology of phase-separated blends are key issues to enhance the efficiency. The nanomorphology of the polymer:fullerene blend is affected by several parameters such as solvent types, casting methods, compositions of donor and acceptor, solution concentration, chemical structure, and last but not least post-production thermal annealing.[5] Initial work on annealing of P3HT:PCBM blend solar cells[6] led to a significantly improved power-conversion efficiency up to 3.5 %.[7] Since then there have been intensive research efforts related to the annealing process.[8–11] Thermal annealing enables crystallization and diffusion of the components in the blend.[11,12] It is well known that an enhanced degree of crystallinity can be induced in polythiophene films by thermal annealing.[13] Furthermore thermal annealing improves the nanoscale morphology[11,14] which can strongly affect the transport pathways for free charges. Annealing also improves the contact to the electron-collecting electrode, and thus collection at the electrodes.[1]

In this work we present a comparative study on the effects involved in the annealing process in "bulk heterojunction" solar-cell devices. We used poly(3-alkylthiophene)s (P3ATs) with different side-chain lengths to systematically distinguish between the two fundamental processes taking place during annealing: a) P3AT crystallization and b) PCBM diffusion. As a result the effect of annealing on these solar-cell devices can be understood in more detail. We show that the extent of PCBM diffusion in these blend films during the annealing process depends on the P3AT side chain length, which is supported by atomic force microscopy (AFM) and optical microscopy results. X-ray diffraction (XRD) measurements allow changes within the blends to be monitored. Thus, the spatial density and size of polymer crystallites in nonannealed and annealed blend films can be determined and compared to the pristine

[*] Dr. L. H. Nguyen, Dr. S. Günes, Prof. N. S. Sariciftci
Linz Institute for Organic Solar Cells (LIOS), Department of Physical Chemistry, Johannes Kepler University Linz
Altenbergerstr. 69, 4040 Linz (Austria)
E-mail: LHnguyen@gmx.at
Dr. H. Hoppe, T. Erb, Prof. G. Gobsch
Institute of Physics, Experimental Physics I
Technical University of Ilmenau
Weimarer Str. 32, 98693 Ilmenau (Germany)
E-mail: harald.hoppe@tu-ilmenau.de

[**] Financial support by the Thuringian Ministry of Culture ("NANORG1" 20101276) is gratefully acknowledged by HH, TE, and GG.

counterparts. Especially interesting in the context of this study are the different unit-cell spacings for the different side-chain lengths in the *a*-axis configuration.[15] Thus a combination of XRD and AFM enables the discrimination between the two contributions taking place during the annealing process: P3AT crystallization and PCBM diffusion.

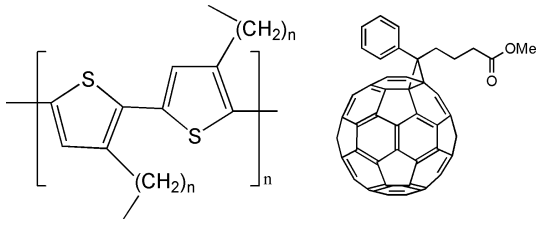

Scheme 1. Chemical structures of P3ATs (left) and PCBM (right).

2. Results and Discussion

The chemical structures of the polyalkylthiophenes applied in this study (poly[3-butyl thiophene] (P3BT), poly[3-hexyl thiophene] (P3HT), poly[3-octyl thiophene] (P3OT), poly[3-decyl thiophene] (P3DT), and poly[3-dodecyl thiophene] (P3DDT) are shown in Scheme 1.

Grazing incidence X-ray diffraction is a useful method for characterizing films of semi-crystalline polymers like P3ATs. Figure 1 displays the XRD results of all investigated P3AT:PCBM blends and pristine P3AT films, both annealed under identical conditions (5 min at 130 °C) and nonannealed. An analysis of the peak positions shows that the interchain spacing for P3ATs in *a*-axis configuration[12] increases gradually with increasing side-chain length: 1.28 nm (P3BT), 1.65 nm (P3HT), 2.05 nm (P3OT), 2.35 nm (P3DT), and 2.6 nm (P3DDT). Consequently, a longer side-chain length leads to an increase in the interspacing between the rigid conjugated backbones. Therefore it can be expected that for a larger spacing the thermally stimulated diffusion of PCBM fullerenes will be less hindered by the conjugated polymer backbones. Furthermore, PCBM can move more freely already during the film-formation process and therefore larger PCBM aggregates in the as-cast blend film may be formed for the longer side-chain polymers.

Interesting to mention are the different XRD peak heights (Fig. 1), representing the spatial number density of the crystal-

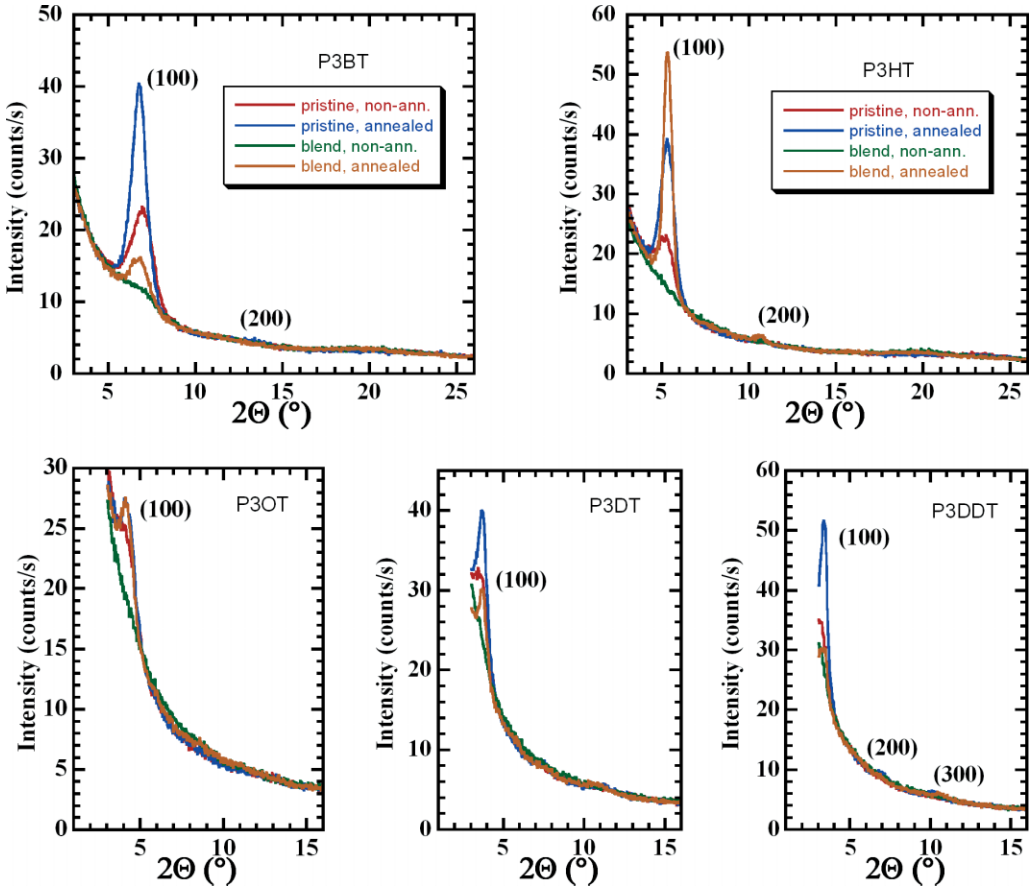

Figure 1. Grazing-incidence XRD diffraction diagrams of pristine P3AT and P3AT:PCBM blend films as-cast and identically annealed: a) P3BT:PCBM, b) P3HT:PCBM, c) P3OT:PCBM, d) P3DT:PCBM, e) P3DDT:PCBM.

ADVANCED FUNCTIONAL MATERIALS

lites. The differences for the various P3ATs have to be related to the annealing temperature in comparison to the crystallite melting temperature. The crystallite melting temperatures for several regioregular P3ATs were determined earlier.[16] Interestingly, the melting temperature decreases for increasing alkyl side-chain lengths. Therefore, the lower peak heights for the polymers with longer side chains have to result from entropy-driven disorder due to a higher mobility of the polymer backbone within the side-chain matrix. This effect can be understood, since for the XRD data shown in Figure 1 all films were treated identically by annealing at 130 °C.

Table 1 shows the photovoltaic properties of solar-cell devices utilizing different side-chain length polyalkylthiophenes without any thermal annealing treatment. We found a monotonic increase of the short-circuit current (I_{SC}) and the power-conversion efficiency (η) for longer alkyl side-chain lengths. To better understand the obtained results, we studied the optical absorption of different P3AT:PCBM blend films in addition.

Table 1. *I–V* characteristics for nonannealed P3AT:PCBM devices.

	I_{SC} [mA cm^{-2}]	V_{OC} [mV]	*FF*	η [%]
P3BT	1.29	300	0.31	0.1
P3HT	1.8	750	0.31	0.42
P3OT	1.97	600	0.38	0.45
P3DT	2.58	550	0.36	0.54
P3DDT	2.9	600	0.38	0.65

Figure 2 shows absorption coefficients of the nonannealed blend films. Here, two things are observable: 1) the absorption coefficient generally decreases for increasing side-chain lengths at the absorption peak position at around 440 nm. This is in accordance with the fact that with shorter side-chains, P3ATs can

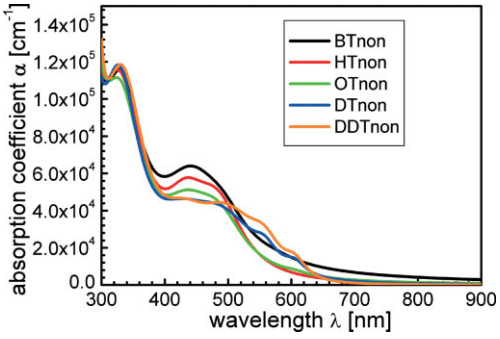

Figure 2. Absorption coefficients of nonannealed P3AT:PCBM blend films.

be packed more closely resulting in a higher density of the light-absorbing backbones, whereas for longer side-chains the volume fraction of alkyl groups, giving no contribution to the absorption of visible light, is larger. 2) The graphs for P3DT and even more for P3DDT show some remarkable structure above 500 nm—already without any annealing. This can be understood by the solvation effect of the side-chains.[17] In general, polymers are better dissolved by the solvent molecules as the length of the side-chains increases. Consequently P3AT chains with longer side-chains have more expanded structures in solution. Furthermore, the increased flexibility and corresponding lower melting temperature of P3AT with longer side-chains enables a higher order to be reached due to faster equilibration in the film. When the number of carbon atoms in the side chain is more than 10, side-chain crystallization even becomes possible.[18,19] The shoulders at 560 and 600 nm represent vibronic progressions and thus reflect an improved crystallinity of the longer side-chain polyalkylthiophenes, corresponding to an improved charge transport of the polymeric phase in blend films. This and the increased lower energy absorption leads to increasing photocurrents for the longer side-chain P3ATs (Table 1).

Figure 3 shows topography images of tapping-mode AFM scans on all as-cast nonannealed thin blend films. Larger aggregates and thus blend phase separation is only found for P3DDT, as can be seen in Figure 3e. In all other blends the scale of phase separation remains considerably smaller than the film thickness and is therefore not observable (compared with previous reports).[20] However, we expect the scale of phase separation to increase generally for longer-side-chain P3ATs, since the fullerene can move more freely there during the film formation because of larger interchain distances. A coarser grained initial intermixing after film formation can lead to better charge-transport properties enabled by a better percolation also of the fullerene phase. This seems to be reflected by slightly improved fill factors for alkyl side-chains larger than six (compare with Table 1).

It is well known that photoactive layers based on P3AT:PCBM blends show dramatically increased performances when a thermal-annealing step is applied after completion of the device. Therefore an optimization concerning the annealing temperature and duration was carried out for each of the P3ATs used. Optimized solar cells (Table 2) show a clear trend in the applied annealing temperature from P3BT to P3DDT: The longer the side-chain the lower the optimal annealing temperature. This is in good accordance with the above-mentioned facts that a) the crystallite melting temperature decreases and b) the ease of fullerene diffusion increases for longer-side-chain P3ATs. Furthermore, in the case of P3DDT we could not detect any significant improvement of the overall power-conversion efficiency due to the thermal-annealing process. We observe that the photocurrents of annealed devices correlate oppositely to the as-cast ones: with increasing side chain lengths the photocurrents are now decreasing. Due to the strong fullerene diffusion in blends with P3ATs having longer side chains, it appears that the system cannot be tuned to the optimal conditions for maximal photocurrents, as the initial phase separation is already too coarse. In general, optimal photocurrent generation requires a trade-off between a maximization of the interfacial area between donor and acceptor and an optimized percolation through the film avoiding charge-carrier recombination losses. The former maximizes the generation of charge carriers, while the percolation directly improves the charge-transport properties.

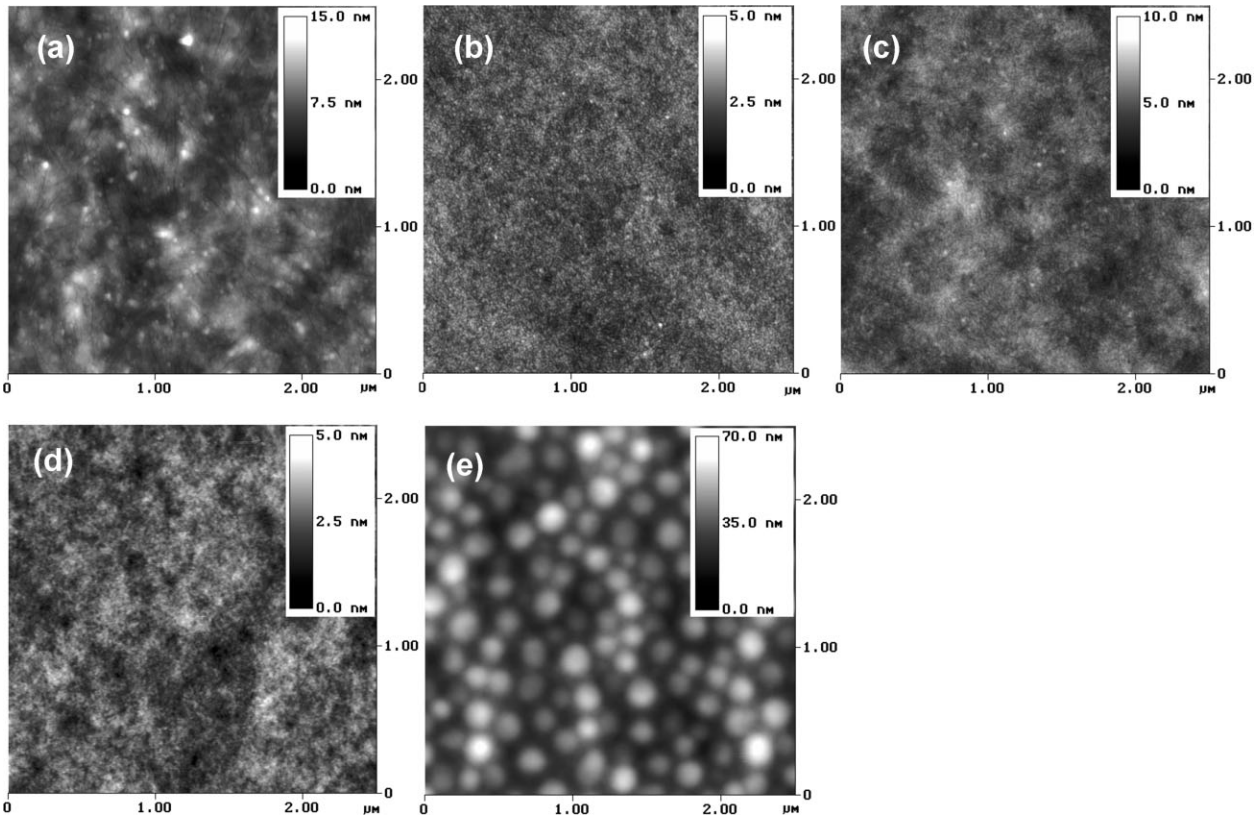

Figure 3. Tapping-mode AFM topography scans of as-cast blend films: a) P3BT:PCBM, b) P3HT:PCBM, c) P3OT:PCBM, d) P3DT:PCBM, e) P3DDT:PCBM.

Table 2. *I–V* characteristics for optimally annealed P3AT:PCBM devices.

	I_{SC} [mAcm^{-2}]	V_{OC} [mV]	*FF*	η [%]	Annealing conditions *T*[°C], time	Melting points [°C]
P3BT	1.87	500	0.29	0.27	160, 30 s	272 [21]
P3HT	6.6	600	0.64	2.55	140, 5 min	240–245 [15b]
P3OT	5.55	500	0.33	0.91	125, 4 min	200–205 [15b]
P3DT	4.22	550	0.45	1.05	75, 5 min	175–180 [15b]
P3DDT	2.9	600	0.38	0.65	none	162 [21]

Transmittance data show that in these optimized annealed P3AT:PCBM blend films strong red shifts and increased absorption (Fig. 4) occur for P3BT, P3HT, and P3OT. Vibronic progressions appear above 500 nm after annealing. This "red-shift" may be assigned to a more flat molecular conformation and thus reduced torsion[22] enabling a better intermolecular order or crystallinity (aggregate state). This higher order will be one reason for the improved solar-cell device characteristics. On the other hand, the increased absorption strength and the generally finer intermixing for shorter side-chain P3ATs is in accordance with the trend in the observed short-circuit photocurrents.

Figure 5 shows AFM images of all P3AT:PCBM blend films annealed at optimized conditions. Except for some increased roughness, the P3BT:PCBM and P3HT:PCBM blends seem not to be affected strongly and no indication of a large-scale phase separation is visible. Remarkably, the P3OT:PCBM and P3DT:PCBM blends show smaller particles in addition to the increased roughness, which may be assigned to small aggregated fullerene crystallites.[8,23–25] The sizes of these aggregates are well below the 100 nm regime, and the blend system is therefore not decomposed.

For comparison, current–voltage (*I–V*) characteristics of nonannealed and optimally annealed ITO/PEDOT/P3AT:PCBM/LiF/Al devices under AM 1.5 illumination are shown in Figure 6. An increase of the fill factors and short-circuit currents is observed upon annealing. However, except for the P3HT-based blend we observe a relatively strong voltage-dependent photocurrent, reflecting severe charge-transport limitations.

To better understand the morphological effects on device performance and to decouple the individual effects of the several processes occurring during device annealing, we treated samples based on the different P3ATs identically at 130 °C for 5 min to enable a direct comparison. The performance of the photovoltaic devices identically annealed for all P3ATs is listed in Table 3. Also in this case we observe the photocurrent to de-

ADVANCED FUNCTIONAL MATERIALS

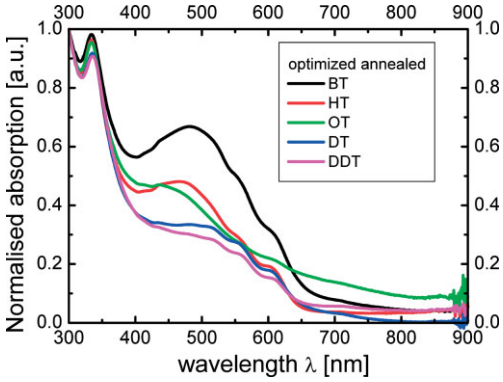

Figure 4. Optical absorption of P3AT:PCBM blend films annealed at optimized conditions.

crease for increasing side-chain length (except for P3BT), however, at this relatively high annealing temperature the photocurrents are smaller for the longer side-chain P3ATs. The reason for the decreasing currents under thermal stress can be related to a too coarse phase separation in the case of longer side-chains, as is elucidated by optical microscopy results in the following.

We observed from Tables 1–3 that upon annealing the V_{OC} reduces, which may be related to changes in the morphology of the active layer of the polymer:fullerene blend. A possible explanation was given by Liu et al.,[26] who stated that the interface composition of polymer and fullerene near the metal contact determines the open circuit voltage. In other words, the V_{OC} is related to the relative amount of polymer and fullerene present at the film surface. In this sense we expect the interface between the photoactive layer and the aluminum to be enriched by PCBM upon annealing, as already proposed by Kim et al.[10]

Table 3. *I–V* characteristics for identically annealed P3AT:PCBM devices at 130 °C, 5 min.

	I_{SC} [mA cm^{-2}]	V_{OC} [mV]	*FF*	η [%]
P3BT	2.08	250	0.33	0.17
P3HT	5.79	550	0.594	1.89
P3OT	3.82	400	027	0.41
P3DT	1.62	450	0.35	0.26
P3DDT	1.40	500	0.41	0.28

Morphological differences in blend films were then measured by tapping-mode AFM as well as in the optical mode to detect larger PCBM crystals. Figure 7 shows a series of AFM images of the identically annealed P3AT:PCBM blends. A morphological destruction expressed by a large-scale phase separation of the P3OT:PCBM, P3DT:PCBM, and P3DDT:PCBM blends can be viewed from optical microscopy. In all of these

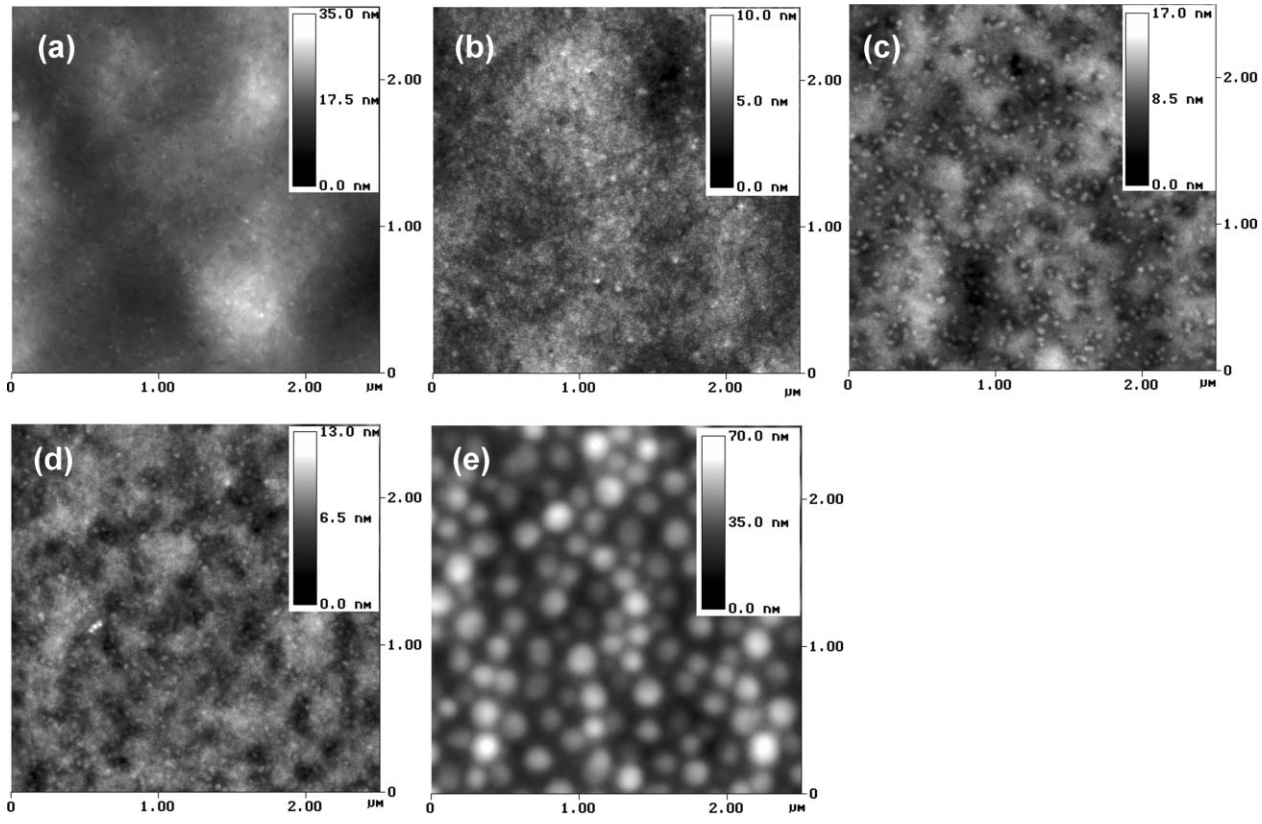

Figure 5. Tapping-mode AFM topography scans of optimally annealed blend films: a) P3BT:PCBM, b) P3HT:PCBM, c) P3OT:PCBM, d) P3DT:PCBM, e) P3DDT:PCBM.

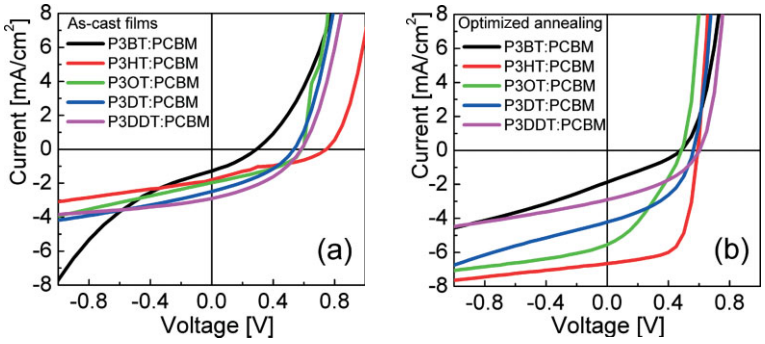

Figure 6. *I–V* characteristics (AM 1.5, 100 mW cm^{-2}) of a) the nonannealed devices and b) optimally annealed devices of P3ATs:PCBM.

films rather large (micrometer-sized) particles become visible under optical microscopy (Fig. 8) and can be assigned to aggregated fullerene crystallites. Thus, the remaining matrix film between those fullerene aggregates almost exclusively consists of the polymer, especially in the case of P3DT and P3DDT. From the given structural information a relatively coarse-grained initial phase separation in the as-cast films can be concluded, as the polymer should not be able to diffuse considerably at these annealing conditions.

In other words, upon heat treatment at 130 °C for 5 min, the fullerene diffusion rate is remarkably increased for the P3OT, P3DT, and P3DDT-based blends when compared to the optimal annealing conditions and therefore results in a larger-scale phase separation. The dependence of the fullerene diffusion rate on the side-chain length and thus the backbone interspacing appears to be directly related to the optimal annealing temperature. Since already in the nonannealed form the phase separation for increasing side-chain lengths is coarser, thermal annealing leads to unfavorable coarse phase separation, although an improved polymeric order is achieved. Furthermore, the unexpected low performance of the P3BT-based device has to be associated with their unsatisfactory dissolving behavior in chloroform.

No PCBM crystallites are observed for P3HT (Fig. 8b), while P3OT (Fig. 8c) shows decomposition for about half of the film. The films based on P3DT and P3DDT are, however, fully decomposed under these annealing conditions. In conclusion, an increasing side-chain length of the polymer enables larger PCBM diffusions rates, which in turn explains the morphological destruction. Consequently, the photocurrent reaches its maximum value for P3HT, and then reduces monotonically for P3ATs carrying larger side-chains like P3OT, P3DT, and P3DDT (Table 3). In general, semicrystalline polymers slow down the diffusion of fullerenes in comparison to amorphous

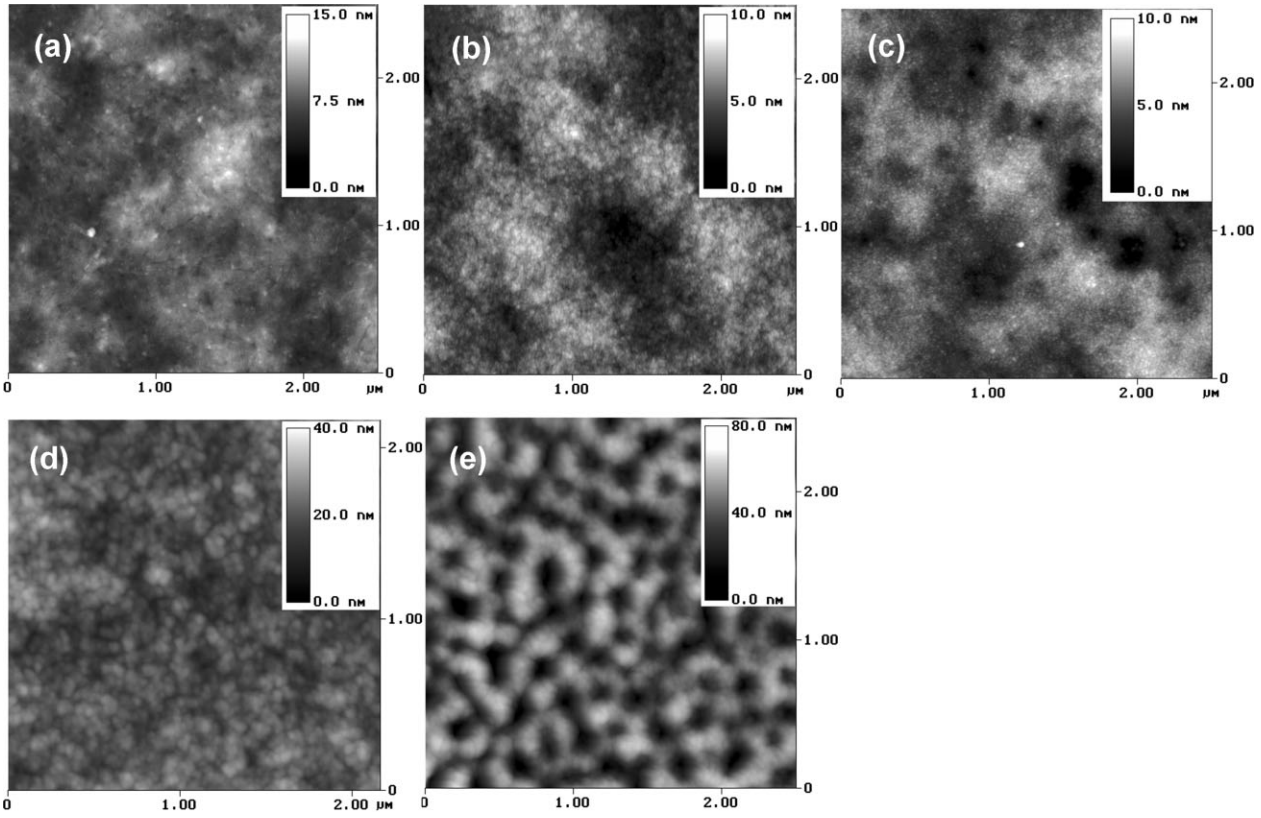

Figure 7. Tapping-mode AFM topography scans of identically annealed blend films: a) P3BT:PCBM, b) P3HT:PCBM, c) P3OT:PCBM, d) P3DT:PCBM, e) P3DDT:PCBM. Scans (d) and (e) are taken from a region of the film that was fully depleted of PCBM.

ADVANCED FUNCTIONAL MATERIALS

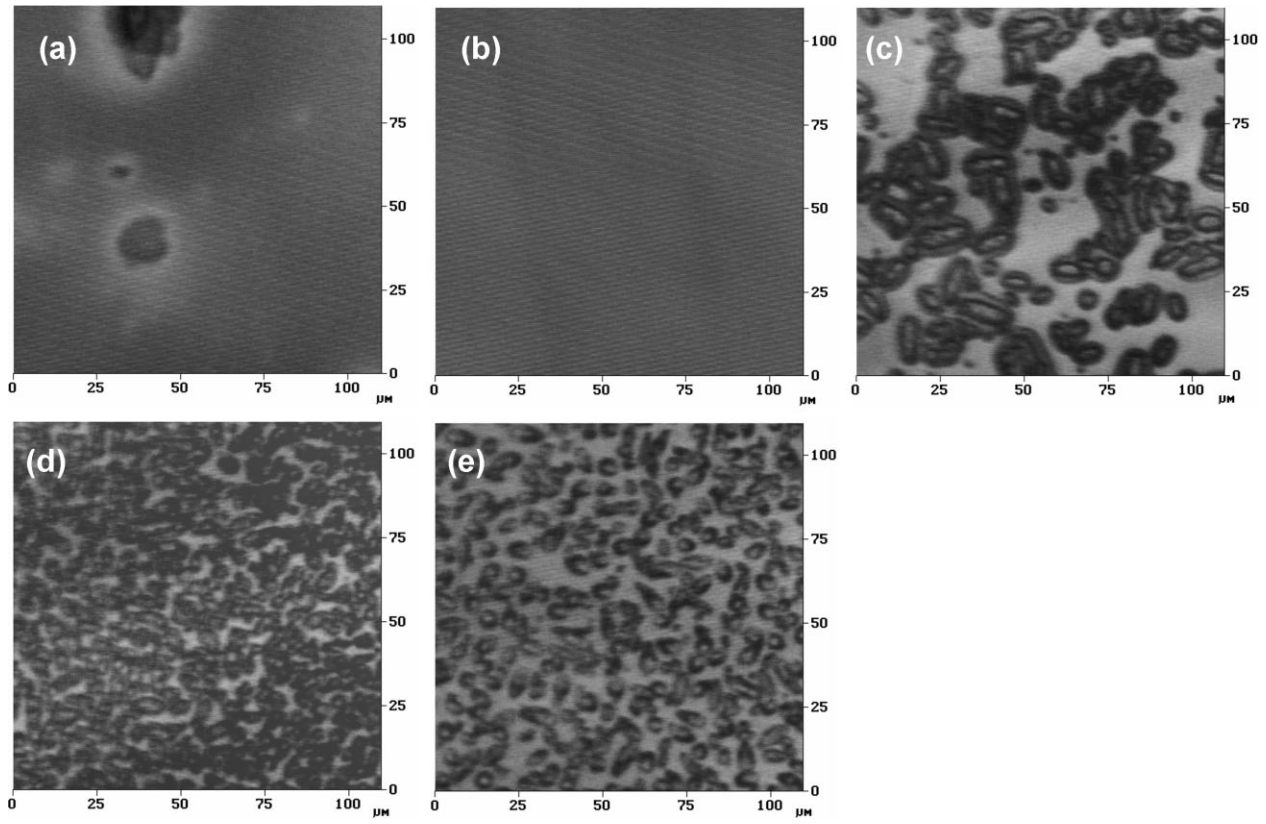

Figure 8. Optical microscopy images of identically annealed blend films: a) P3BT:PCBM, b) P3HT:PCBM, c) P3OT:PCBM, d) P3DT:PCBM, e) P3DDT:PCBM. The micrometer-sized particles in (c–e) are crystalline PCBM aggregates.

polymers due to the formation of higher density fibrillar crystallites.[11] Here we find that if the side-chain length becomes too long, this advantage disappears again.

Taking the XRD and AFM results together makes one point clear: the rapid PCBM diffusion is the main limiting parameter in the blend films during the annealing process.

3. Conclusions

Optimal post-production annealing requires a fine adjustment for every P3AT:PCBM combination to provide for the two main morphological effects: 1) enhancement of P3AT crystallinity, leading to increased absorption and improved charge-carrier transport, and 2) diffusion of the PCBM leading to an increase of the phase separation. In conclusion, longer side-chain lengths of poly(3-alkylthiophenes) enable higher diffusion rates of PCBM in the polymer matrix leading ultimately to a larger scale of phase separation, both directly after film formation and especially after the thermal annealing step. This significantly decreases the performance of photovoltaic devices due to a reduced interfacial area and, thus, less photocurrent generation. Further aspects for smaller photocurrents from the longer side-chain P3ATs are the reduced volume density of light-absorbing backbones.

4. Experimental

Materials: Regioregular poly(3-butylthiophene) (P3BT), poly(3-hexylthiophene) (P3HT), poly(3-octylthiophene) (P3OT), poly(3-decylthiophene) (P3DT), and poly(3-dodecylthiophene) (P3DDT) (Scheme 1, left) were purchased from Aldrich Chemical Co. The materials were synthesized by the Rieke method. The HT (HT = head-to-tail) regioregularity reported by the company was > 97 % for P3BT and > 98.5 % for P3HT, P3OT, P3DT, and P3DDT. The molecular weights were reported as: P3HT ($M_w = 37\,680$, $M_n = 25\,500$), P3OT ($M_w = 39\,210$, $M_n = 34\,580$), P3DT ($M_w = 42\,220$, $M_n = 30\,480$), and P3DDT ($M_w = 49\,210$, $M_n = 34\,650$). 1-(3-methoxycarbonylpropyl)-1-phenyl-[6,6]C_{61} (PCBM) is shown in Scheme 1 (right).

Solar-Cell Fabrication: Solar-cell devices were prepared from 1 wt % solutions of the polymer and PCBM at weight ratios of 1:2 using chloroform as solvent. Poly(3,4-ethylene dioxythiophene):poly(styrene sulfonate) (PEDOT:PSS) (Baytron PH, Bayer Germany) was spin-coated on top of indium-tin oxide (ITO) (Merck, Germany) coated glass (ca. 25 Ω/sq) which had been cleaned in an ultrasonic bath with acetone and isopropyl alcohol. The active layer was spin-coated on the PEDOT:PSS layer. Then 6 Å of lithium fluoride (LiF) and an 80 nm thick Al electrode was deposited onto the blend film by thermal evaporation at ca. 5×10^{-6} mbar. All current–voltage (*I–V*) characteristics of the photovoltaic devices were measured under inert atmosphere (argon) in a dry glove box using a Keithley SMU 2400 unit. A Steuernagel solar simulator was used as the excitation source with a power of 100 mW cm^{-2} white light illumination (AM 1.5 conditions).

AFM: Atomic force microscopy studies were performed using a Digital Instruments Dimension 3100 in the tapping mode. The AFM characterization was performed on an area of the active layer of the photovoltaic device where the electrode was not deposited.

XRD: XRD measurements were performed using a Philips X'Pert-Pro diffractometer. The thin films were studied in grazing-incidence diffraction (GID) geometry to increase the effective X-ray path length for scattering in the P3AT:PCBM layers. The angle between film surface and incident beam was fixed at 0.3°. As radiation source a monochromatic Cu Kα beam with a wavelength of $\lambda = 0.154$ nm was applied. The detector scans at the angle 2θ in a plane defined by the incident beam and the surface normal.

Received: November 1, 2006
Revised: December 29, 2006
Published online: March 12, 2007

[1] W. Ma, C. Yang, X. Gong, K. Lee, A. J. Heeger, *Adv. Funct. Mater.* **2005**, *15*, 1617.
[2] G. Yu, J. Gao, J. C. Hummelen, F. Wudl, A. J. Heeger, *Science* **1995**, *270*, 1789.
[3] N. S. Sariciftci, L. Smilowitz, A. J. Heeger, F. Wudl, *Science* **1992**, *258*, 1474.
[4] C. D. Dimitrakopoulos, D. J. Mascaro, *IBM J. Res. Dev.* **2001**, *45*, 11.
[5] H. Hoppe, N. S. Sariciftci, *J. Mater. Chem.* **2006**, *16*, 45.
[6] N. Camaioni, G. Ridolfi, G. Casalbore-Miceli, G. Possamai, M. Maggini, *Adv. Mater.* **2002**, *14*, 1735.
[7] F. Padinger, R. S. Rittberger, N. S. Sariciftci, *Adv. Funct. Mater.* **2003**, *13*, 85.
[8] D. Chirvase, J. Parisi, J. C. Hummelen, V. Dyakonov, *Nanotechnology* **2004**, *15*, 1317.
[9] H. Hoppe, N. Arnold, D. Meissner, N. S. Sariciftci, *Thin Solid Films* **2004**, *451–452*, 589.
[10] Y. Kim, S. A. Choulis, J. Nelson, D. D. C. Bradley, S. Cook, J. R. Durrant, *Appl. Phys. Lett.* **2005**, *86*, 063 502.
[11] X. Yang, J. Loos, S. C. Veenstra, W. J. H. Verhees, M. M. Wienk, J. M. Kroon, M. A. J. Michels, R. A. J. Janssen, *Nano Lett.* **2005**, *5*, 579.
[12] T. Erb, U. Zhokhavets, G. Bobsch, S. Raleva, B. Stuehn, P. Schilinsky, C. Waldauf, C. J. Brabec, *Adv. Funct. Mater.* **2005**, *15*, 1193.
[13] Y. Zhao, G. X. Yua, P. Roche, M. Leclerc, *Polymer* **1995**, *36*, 2211.
[14] G. Li, V. Shrotriya, J. Huang, Y. Yao, T. Moriarty, K. Emery, Y. Yang, *Nat. Mater.* **2005**, *4*, 864.
[15] a) T. J. Prosa, M. J. Winokur, J. Moulton, P. Smith, A. J. Heeger, *Macromolecules* **1992**, *25*, 4364. b) T. Chen, X. Wu, R. D. Rieke, *J. Am. Chem. Soc.* **1995**, *117*, 233. c) K. E. Aasmundtveit, E. J. Samuelsen, M. Guldstein, C. Steinsland, O. Flornes, C. Fagermo, T. M. Seeberg, L. A. A. Pettersson, O. Inganäs, R. Feidenhans, L. S. Ferrer, *Macromolecules* **2000**, *33*, 3120.
[16] C. Yang, F. P. Orfino, S. Holdcroft, *Macromolecules* **1996**, *29*, 6510.
[17] C.-K. Shin, H. Lee, *Synth. Met.* **2004**, *140*, 177.
[18] V. Causin, C. Marega, A. Marigo, *Macromolecules* **2005**, *38*, 409.
[19] S. Malik, A. K. Nandi, *J. Polym. Sci., Part B Polym. Phys.* **2002**, *40*, 2073.
[20] H. Hoppe, M. Niggemann, C. Winder, J. Kraut, R. Hiesgen, A. Hinsch, D. Meissner, N. S. Sariciftci, *Adv. Funct. Mater.* **2004**, *14*, 1005.
[21] K. Yazawa, Y. Inoue, T. Yamamoto, N. Asakawa, *Phys. Rev. B* **2006**, *74*, 094 204.
[22] J. Roncali, *Chem. Rev.* **1997**, *97*, 173.
[23] X. Yang, J. K. J. van Duren, R. A. J. Janssen, M. A. J. Michels, J. Loos, *Macromolecules* **2004**, *37*, 2151.
[24] M. Drees, H. Hoppe, C. Winder, H. Neugebauer, N. S. Sariciftci, W. Schwinger, F. Schaeffler, C. Topf, M. C. Scharber, Z. Zhud, R. Gaudianad, *J. Mater. Chem.* **2005**, *15*, 5158.
[25] H. Hoppe, M. Dress, W. Schwinger, F. Schaeffler, N. S. Sariciftci, *Synth. Met.* **2005**, *152*, 117.
[26] J. Liu, Y. Shi, Y. Yang, *Adv. Funct. Mater.* **2001**, *11*, 420.